

NANO EXPRESS

Open Access



Optical Properties and Growth Mechanism of $\text{La}_3\text{Ga}_{5.5}\text{Nb}_{0.5}\text{O}_{14}$ Macroporous Ceramic

Yu-Jen Hsiao^{*} , Yempati Nagarjuna and Sheng-Chang Wang

Abstract

Optical properties and growth mechanism of $\text{La}_3\text{Ga}_{5.5}\text{Nb}_{0.5}\text{O}_{14}$ oxides by a Pechini process were investigated. The structure and morphology were obtained after sintering at 600–800 °C. This crystallized orthorhombic $\text{La}_3\text{Ga}_{5.5}\text{Nb}_{0.5}\text{O}_{14}$ can be obtained by the heat treatment process at 800 °C from XRD. A proposed schematic growth mechanism of $\text{La}_3\text{Ga}_{5.5}\text{Nb}_{0.5}\text{O}_{14}$ macroporous based on the details provided is shown. The photo-luminescence spectra shown that under 327 nm excitation spectra, a broad and blue emission peak is observed at 475 nm at 77 K and this spectrum is originated from the $[\text{NbO}_6]^{7-}$ octahedra group. The optical absorption spectra of the 800 °C sample exhibited a well-crystalline and very low oxygen vacancy, which corresponded to the band gap energies of 3.95 eV.

Keywords: $\text{La}_3\text{Ga}_{5.5}\text{Nb}_{0.5}\text{O}_{14}$, Macroporous, Optical properties, Pechini process

Introduction

The piezoelectric and optical properties of $\text{Ca}_3\text{Ga}_2\text{Ge}_4\text{O}_{14}$ (CGG)-type structure of $\text{La}_3\text{Ga}_5\text{SiO}_{14}$ (LGS) [1], $\text{La}_3\text{Ga}_{5.5}\text{Nb}_{0.5}\text{O}_{14}$ (LGN) [2], and $\text{La}_3\text{Ga}_{5.5}\text{Ta}_{0.5}\text{O}_{14}$ (LGT) [3] compounds have been actively and systematically studied. They have been investigated for bulk acoustic wave (BAW) and surface acoustic wave (SAW) devices for the fabrication of filters with large pass bandwidths and oscillators with a large shift or high-frequency stability [4–7]. The piezoelectric and dielectric oxide has been applied in the optical field [8, 9]. A promising nonlinear oxide crystal $\text{La}_3\text{Ga}_{5.5}\text{Nb}_{0.5}\text{O}_{14}$ (LGN) is proposed and fully characterized in recent years. The mid-infrared spectral range extending from 2 to 6 μm is significant for scientific and technological applications [10]. The phase-matching angles of second-harmonic generation and difference-frequency generation up to 6.5 μm was also measured in the langanate crystal $\text{La}_3\text{Ga}_{5.5}\text{Nb}_{0.5}\text{O}_{14}$ (LGN) [11]. Voda et al. [12] reported that it was used both as a laser and a laser host material. Nd: $\text{La}_3\text{Ga}_{5.5}\text{Nb}_{0.5}\text{O}_{14}$ laser properties of output power and wavelength temperature tuning under laser diode pumping are also verified [13].

Macroporous materials have porosity ranging from 5 to 90% and pore size ranging more than 100 nm. Macroporous materials have diverse properties like excellent

mechanical strength, high thermal conductivity, good chemical resistance, and high thermal shock resistance which led into the industrial applications like filtration for water and gas, thermoelectric convertor, catalytic agent [14]. Due to photonic band gaps, macroporous photonic crystals have been used for advanced applications such as optical communications, light emissions, and gas sensing. Macroporous photonic crystals of different materials can be used in chemical detections, and this led to explore different macroporous materials for gas sensing. Porous ceramics are of great interest due to their numerous potential applications in industries such as catalysis, adsorption and separation, filtration of molten metals or hot gases, refractory insulation of furnaces, and hard tissue repair and engineering [15].

Recently, very few works have been done on LGN-based macroporous ceramic formed by the chemical method. Yu [16] prepared piezoelectric crystal of $\text{La}_3\text{Ga}_{5.5}\text{Nb}_{0.5}\text{O}_{14}$ by using the sol-gel process and examined microstructure analysis. The results have shown that LGN nanoparticles were crystallized in the trigonal crystallographic phase. Kong [17] studied the growth of single-crystal $\text{La}_3\text{Ga}_{5.5}\text{Nb}_{0.5}\text{O}_{14}$ (LGN) by the Czochralski method which requires high temperature such as more than 1500 °C. In our study, macroporous polycrystal was developed by using the Pechini process which requires low temperature such as 800 °C. The polycrystal and the single crystal have the same

* Correspondence: yujenshao.tw@gmail.com

Department of Mechanical Engineering, Southern Taiwan University of Science and Technology, Tainan 710, Taiwan

orthorhombic phase. The main purpose of this work is to use a Pechini process for the preparation of a single-phase $\text{La}_3\text{Ga}_{5.5}\text{Nb}_{0.5}\text{O}_{14}$ LGN ceramic with the calcium-gallogermanate (CGC-type) structure (trigonal, space group P321) [18]. The major advantage of the Pechini process is that there is a low-temperature processing [19–21]. Chemically synthesized ceramic powders often possess better chemical homogeneity and better size control of particle morphology than those produced by the mixed oxide route [22]. Therefore, the optical properties and growth mechanism of LGN macroporous oxide have been investigated in this study.

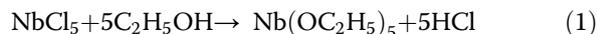
Methods/Experimental

Materials Used

Lanthanum nitrate $\text{La}(\text{NO}_3)_3$, gallium nitrate $\text{Ga}(\text{NO}_3)_3$, niobium chloride (NbCl_5), citric acid anhydrous (CA), and ethylene glycol (EG).

Preparation of $\text{La}_3\text{Ga}_{5.5}\text{Nb}_{0.5}\text{O}_{14}$

The $\text{La}_3\text{Ga}_{5.5}\text{Nb}_{0.5}\text{O}_{14}$ macroporous ceramics were prepared by the Pechini process using lanthanum nitrate $\text{La}(\text{NO}_3)_3$, gallium nitrate $\text{Ga}(\text{NO}_3)_3$, niobium chloride (NbCl_5), citric acid anhydrous (CA), and ethylene glycol (EG). All materials have over 99.9% purities. According to the reaction, niobium ethoxide, $\text{Nb}(\text{OC}_2\text{H}_5)_5$ synthesis takes place from niobium chloride NbCl_5 and ethanol, $\text{C}_2\text{H}_5\text{OH}$.



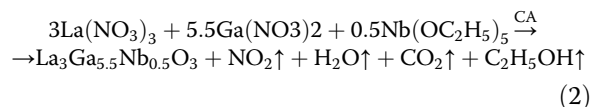
The stoichiometric amount of lanthanum nitrate, gallium nitrate, and niobium ethoxide was dissolved in water. A chelating agent such as citric acid is added to the solution. The molar ratio of citric acid and metal ions used in this process is 2:1. A stabilizing agent such as ethylene glycol is added to the above solution. The precursor containing La, Ga, and Nb were dried in an oven at 120 °C for 24 h, and then, the $\text{La}_3\text{Ga}_{5.5}\text{Nb}_{0.5}\text{O}_{14}$ ceramics were obtained after sintering at 600–800 °C for 3 h in air.

Characterization/Phase Identification

The burnout behaviors of powders were analyzed by differential thermal analysis and thermogravimetry analysis (DTA–TGA, PE–DMA 7). The phase identification was performed by X-ray powder diffraction (Rigaku Dmax-33). The morphology and microstructure were examined by transmission electron microscopy (HR-TEM, HF-2000, Hitachi). The excitation and emission spectra were recorded on a Hitachi-4500 fluorescence spectrophotometer equipped with xenon lamp at 300 K and 77 K. The absorption spectra were measured using a Hitachi U-3010 UV–vis spectrophotometer at room temperature.

Results and Discussion

The amorphous compound is subjected to heat treatment to undergo pyrolysis process to become crystalline structure. In this experiment, the possible chemical reactions for the synthesis of $\text{La}_3\text{Ga}_{5.5}\text{Nb}_{0.5}\text{O}_3$ powders can be expressed as follows:



This precursor powder is heat-treated for about 3 h at 600–800 °C, and the XRD patterns for this temperature are shown in Fig. 1. At 600 °C calcined temperature, the precursor powder has shown its small amount of microcrystal structure. When the temperature raised to 700 °C, decomposition of amorphous powder takes place and it begins to crystallize. When the sintered temperature reaches 800 °C, the precursor powder sample is shown in a single phase which is orthorhombic $\text{La}_3\text{Ga}_{5.5}\text{Nb}_{0.5}\text{O}_{14}$ phase (JCPDS file no. 47-0533) where the peaks are identified. This sharper peak shows that the crystalline form of the $\text{La}_3\text{Ga}_{5.5}\text{Nb}_{0.5}\text{O}_{14}$ powder. With the increase in temperature, the intensity of the peaks becomes sharper which indicates the crystalline structure of the $\text{La}_3\text{Ga}_{5.5}\text{Nb}_{0.5}\text{O}_{14}$ powder.

The FT-IR spectra of the powder at 600–800 °C are shown in Fig. 2. Figure 2a, b shows the IR spectra of

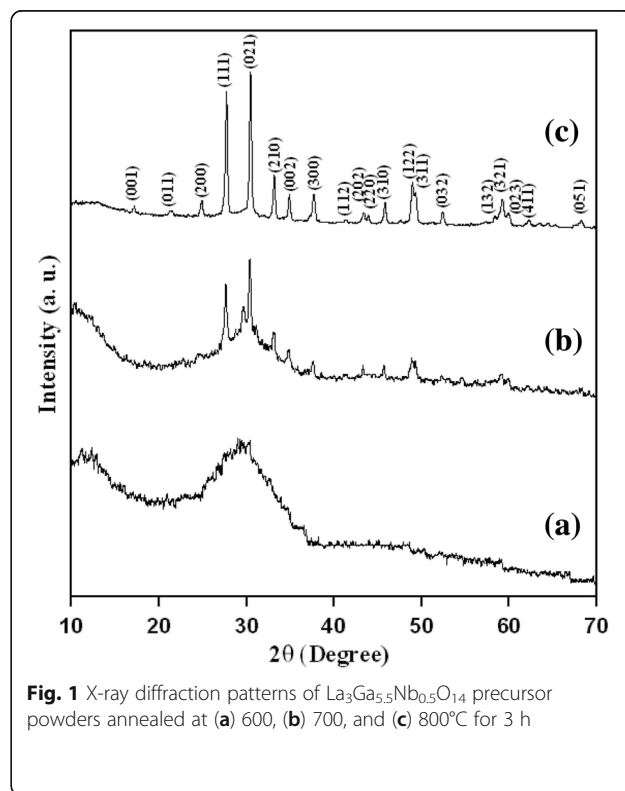
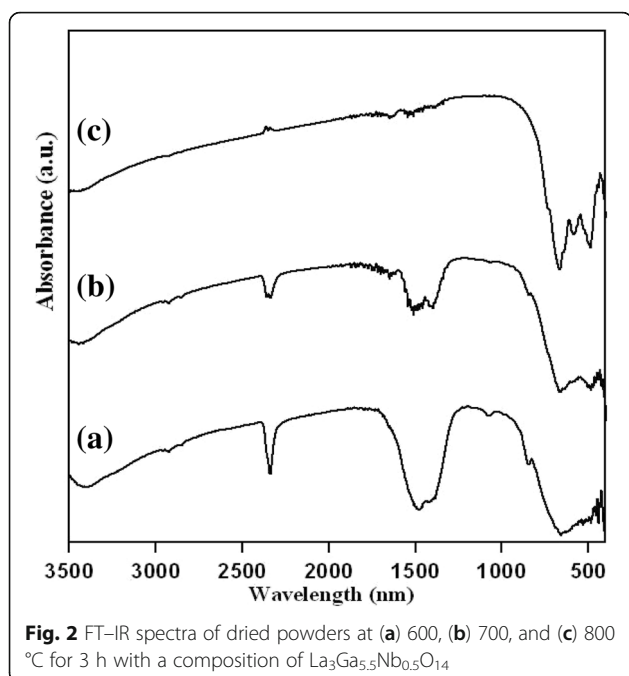


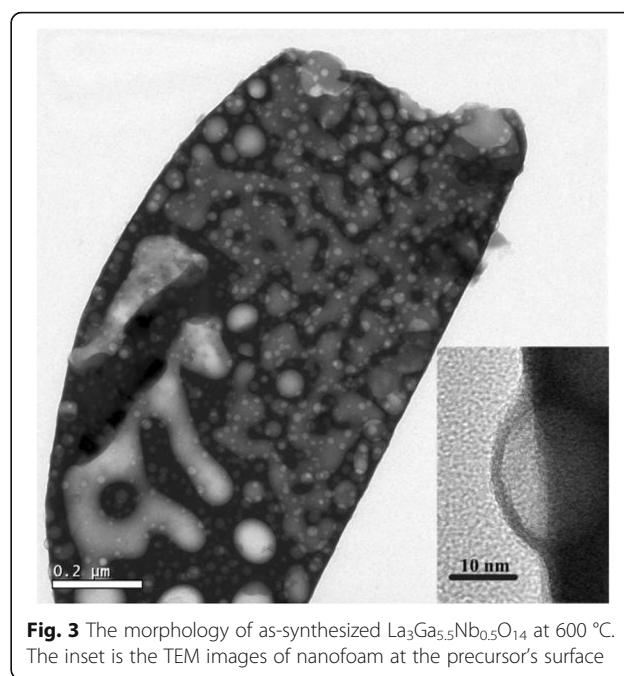
Fig. 1 X-ray diffraction patterns of $\text{La}_3\text{Ga}_{5.5}\text{Nb}_{0.5}\text{O}_{14}$ precursor powders annealed at (a) 600, (b) 700, and (c) 800°C for 3 h



powder at 600 to 700 °C, respectively, where there is a sharp stretch at 2300 nm wavelength which identifies the presence of strong carbon dioxide compound class stretching and there is a bulk stretch at 1500 nm wavelength which indicates the absorbed nitrate ions in the structure [14]. So, these might be the strong stretching vibrations of nitrate ions. From Fig. 2c, there are new peaks formed at 500 to 600 nm when the annealing temperature is increased to 800 °C. This new peak indicates the formation of the $\text{La}_3\text{Ga}_{5.5}\text{Nb}_{0.5}\text{O}_{14}$ nanocrystals. The peaks present at 1500 nm and 2300 nm wavelength are calcined at 800 °C. This shows the presence of little residues in the organic compound.

TEM images of the precursor powder at 600 °C for the morphology are shown in Fig. 3. The first image shows the size and shape morphology of the precursor ceramic. From the figure, different sizes of nanofoams are present in the precursor powder. The second image is the enlarged version and side view of the first image. It is shown that bulged nanofoams are present on the surface of the precursor at the beginning of crystal formation. These nanofoams are of different sizes as seen from the image. These nanofoams have a low thickness, and when the temperature increases, these nanofoams form microporous holes. This shows the particles have a semi-circular shape which is hollow inside. This nanoporous material is a nanofoam which contains gas inside of it. When the temperature will increase, these nanofoams will leave a hole of diameter less than 100 nm.

TEM images of different magnification is showed in Fig. 4. In the Fig. 4(a), the magnification is very low which is 100 nm and the structure visibility is not good.



In Fig. 4(b) the TEM image is magnified to 10 nm and crystal structure can be seen. In Fig. 4(c) image is enlarged to 5 nm. Fig. 4(d) represents the small amount of micro crystal structure.

TEM analysis for the crystal at 800 °C is shown in Fig. 5. The first Fig. 5a magnification is very low which shows the nanocomposition of the crystal form. Figure 5b is a highly magnified image of the crystal where the structure of the macroporous crystal is seen. The bright images are the air holes which are formed from the nanofoams. Electron diffraction of the $\text{La}_3\text{Ga}_{5.5}\text{Nb}_{0.5}\text{O}_{14}$ crystalline structure is shown in Fig. 5c. There are circular bright continuous rings in the electron diffraction pattern. This indicates that the particles were nanosized, and it also confirms the crystalline nature of the nanoparticles [23]. EDX analysis of $\text{La}_3\text{Ga}_{5.5}\text{Nb}_{0.5}\text{O}_{14}$ macroporous oxide is shown in Fig. 5d. This analysis shows about the molar ratio of the structure $\text{La}_3\text{Ga}_{5.5}\text{Nb}_{0.5}\text{O}_{14}$. The peak of Ga is high which indicates it has more content. Nb has a very low peak since it is very less in content.

A proposed schematic growth mechanism of $\text{La}_3\text{Ga}_{5.5}\text{Nb}_{0.5}\text{O}_{14}$ macroporous based on the details provided is shown in Fig. 6. In this process, synthesized macroporous oxide forms crystals at 600 °C as shown in the schematic Fig. 5a. As mentioned, the precursor powder is at 600 °C, and it has nanofoams which are nanostructured porous materials with diameters less than 100 nm. These nanofoams are bulk nanoporous materials with enlarged form and very low thickness. The formation of nanofoams takes place because of heating in the presence of oxygen. At this stage, the precursor is in non-crystalline

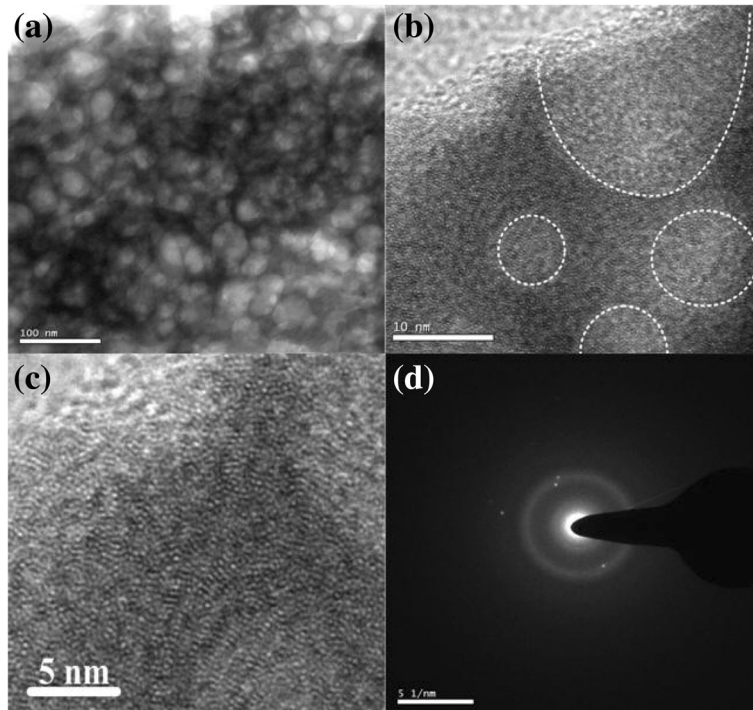


Fig. 4 **a** TEM images of as-synthesized $\text{La}_3\text{Ga}_{5.5}\text{Nb}_{0.5}\text{O}_{14}$ at 700 °C, **b** high-resolution TEM image of the microporous, **c** the lattice image for short-range order nanocrystalline structure, and **d** electron diffraction pattern of the short-range order nanocrystalline area

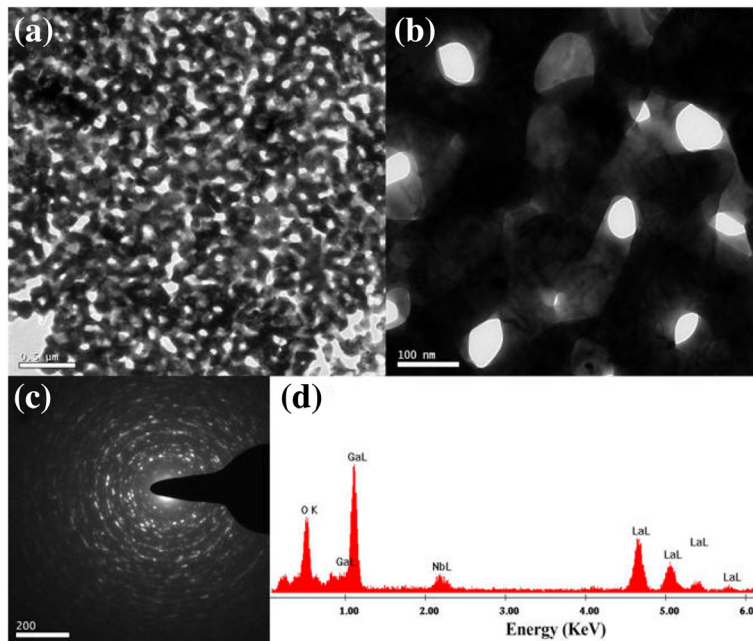


Fig. 5 **a** TEM images of as-synthesized macroporous at 800 °C, **b** high-resolution TEM image of the macroporous, **c** electron diffraction pattern, and **d** EDX analysis of $\text{La}_3\text{Ga}_{5.5}\text{Nb}_{0.5}\text{O}_{14}$ macroporous oxide

form. When the annealing temperature is increased to 700 °C, the bulky nanofoams will pop-out due to less thickness, and it leaves a hole of diameter less than 100 nm. These nanofoams are bulk nanoporous materials which are filled with either liquid or gas. In this case, these nanofoams are filled with gas either oxygen or carbon dioxide. At this stage, the precursor is in non-crystalline form. When the annealing temperature is increased to 700 °C, these nanofoams which are hollow inside will pop-out leaving a hole of diameter less than 100 nm. During the 600 to 700 °C annealing process, these nanofoams tend to grow size bigger and eventually form macroporous holes. At the same time, a lot of microcrystals are formed in an irregular order around the nanofoam holes. After the nanofoams collapsed and sintering occurred, the grain size will grow and inter-facial energy will be decreased [24] (Fig. 6).

When the annealing temperature is increased to 800 °C, the microcrystals form into crystal grains which are hard, and these grains are separated by the boundary grains. In this process, the collapse rate of nanofoams is directly proportional to the crystallization process. If the calcined temperatures are increased, it encourages the growth of the oxide crystals. The structure formed will be crystallized, and the macroporous holes will be formed which are of different sizes ranging from 50 to 100 nm.

The emission spectra of the $\text{La}_3\text{Ga}_{5.5}\text{Nb}_{0.5}\text{O}_{14}$ samples at 77 K and 300 K are shown in Fig. 7. Photo-luminescence results show that the sample prepared at 77 K have

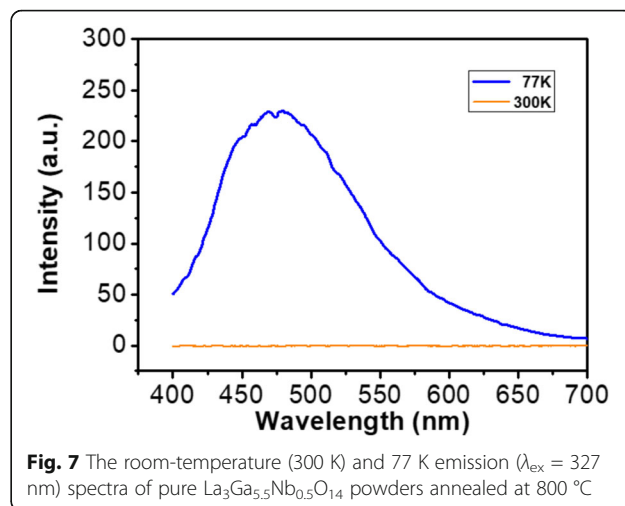


Fig. 7 The room-temperature (300 K) and 77 K emission ($\lambda_{\text{ex}} = 327$ nm) spectra of pure $\text{La}_3\text{Ga}_{5.5}\text{Nb}_{0.5}\text{O}_{14}$ powders annealed at 800 °C

exhibited emission spectra at 475 nm than the sample at room temperature 300 K. The ideal state temperature for the sample is 77 K, and at this temperature, there will be no thermal vibrations which affect the procedure. According to Blasse [25], there are two kinds of absorbing groups in niobate complexes which are $[\text{NbO}_6]^{7-}$ and $[\text{NbO}_4]^{3-}$. At 327 nm excitation spectra, there was only one peak appeared which corresponds to the $[\text{NbO}_6]^{7-}$ complex group. This indicates that the charge transfer happened in the bands of $[\text{NbO}_6]^{7-}$ in the $\text{La}_3\text{Ga}_{5.5}\text{Nb}_{0.5}\text{O}_{14}$ system. So here, the crystal structure of $\text{La}_3\text{Ga}_{5.5}\text{Nb}_{0.5}\text{O}_{14}$ might be built up by the edge-sharing of NbO_6 trigonal prisms.

The PL emission spectra showed a strong blue emission spectra peak at 457 nm. Here, the luminescence

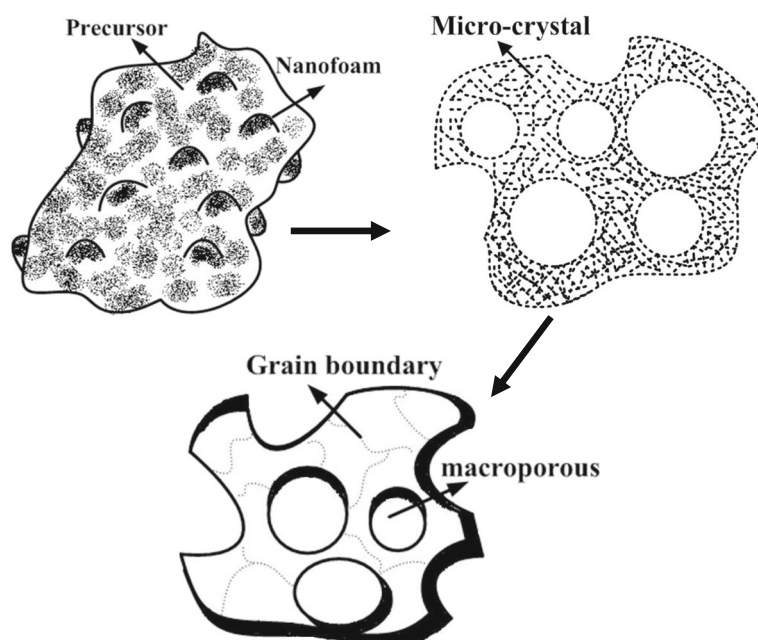


Fig. 6 The schematic mechanism for the growth of $\text{La}_3\text{Ga}_{5.5}\text{Nb}_{0.5}\text{O}_{14}$ macroporous via a sol-gel route in our specially designed precursor solution

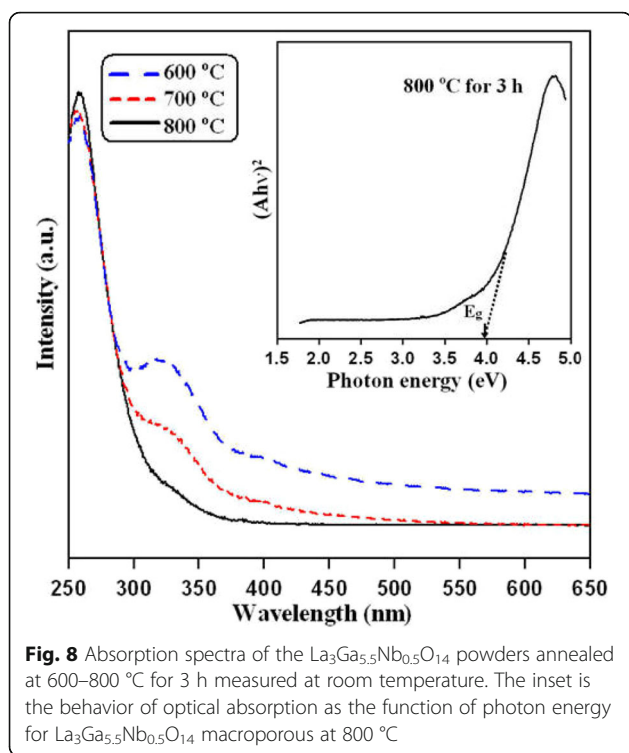


Fig. 8 Absorption spectra of the $\text{La}_3\text{Ga}_{5.5}\text{Nb}_{0.5}\text{O}_{14}$ powders annealed at 600–800 °C for 3 h measured at room temperature. The inset is the behavior of optical absorption as the function of photon energy for $\text{La}_3\text{Ga}_{5.5}\text{Nb}_{0.5}\text{O}_{14}$ macroporous at 800 °C

effect depends on the Nb–O–Nb bonding where the conduction band consists of Nb^{5+} 4d orbitals and the valance band of O^{2-} 2p orbitals between the corner-sharing octahedral [26]. A strong temperature dependence of the emission peak was observed. The intensity of the emission peak reduced rapidly and nearly disappears when the temperature increased from 77 to 300 K. The quenching of the emission peak should be attributed to two reasons for thermal quenching effect in macroporous $\text{La}_3\text{Ga}_{5.5}\text{Nb}_{0.5}\text{O}_{14}$ ceramic. The one is that non-radiative transition results in the heat by transfer of energy to phonons in the lattices; another one is that the electrons could be trapped by any possible defects in the lattices; and it is well known that the trap centers in niobate complexes, which could have an important quenching effect on luminescence [27, 28].

UV-Vis absorption spectra of the $\text{La}_3\text{Ga}_{5.5}\text{Nb}_{0.5}\text{O}_{14}$ macroporous particles are measured, and band gap is estimated from the absorption spectra in Fig. 8. The absorption luminescence has a maximum intensity of 260 nm which corresponds with the excitation spectra. The absorbance in the vicinity of the onset due to the electronic transition for a given semiconductor is given by the following equation:

$$\alpha = \frac{C(h\nu - E_g)^{1/2}}{h\nu} \quad (3)$$

where α is the absorption coefficient, C is the constant, $h\nu$ is the photon energy, and E_g is the band gap. The inset of Fig. 8 shows the relationship of $(\alpha h\nu)^2$ and $h\nu$. The inset in Fig. 8 shows the band gap of 3.95 eV. In the experiment, there are little bumps present at about 320 nm from 600 to 800 °C. These bumps indicate the presence of oxygen vacancy defect [29]. At 800 °C annealing temperature, the organic compound fiercely burnt very rapidly, and this consumed a great amount of oxygen. It is also noted that the defects are high at 600 °C, and with the increase in temperature, these vacancy defects are reduced.

Conclusions

$\text{La}_3\text{Ga}_{5.5}\text{Nb}_{0.5}\text{O}_{14}$ macroporous polycrystal is prepared by a Pechini process using NbCl_5 , $\text{Ga}(\text{NO}_3)_3$, and $\text{La}(\text{NO}_3)_3$. This crystallized orthorhombic $\text{La}_3\text{Ga}_{5.5}\text{Nb}_{0.5}\text{O}_{14}$ can be obtained by the heat treatment process at 800 °C from XRD. The excitation wavelength is about 327 nm, and this is associated with charge transfer bands of Nb^{5+} and O^{2-} ions in a tetrahedral co-ordination. The photo-luminescence spectra shown that under 327 nm excitation spectra, a broad and blue emission peak is observed at 475 nm and this spectrum is originated from the $[\text{NbO}_6]^{7-}$ octahedra group. The visible light absorption edge of 800 °C sample was at 320 nm, which corresponded to the band gap energies of 3.95 eV.

Abbreviations

BAW: Bulk acoustic wave; CA: Citric acid; CGC: Calciumgallogermanate; DTA: Differential thermal analysis; EDX: Energy dispersive X-ray analysis; E_g : Band gap; EG: Ethylene glycol; FTIR: Fourier-transform infrared spectroscopy; $h\nu$: Photon energy; PL: Photoluminescence; SAW: Surface acoustic wave; TEM: Transmission electron microscopy; TGA: Thermogravimetry analysis; UV-vis: Ultraviolet-visible; XRD: X-ray powder diffraction

Acknowledgements

We thank the Taiwan Semiconductor Research Institute (TSRI) and Professor Guo-Ju Chen from I-Shou University for technical support.

Authors' contributions

YJH initiated the idea of the experiment and conducted the experiment. YN and SCW helped with the results and discussion. YJH, YN, and SCW collectively wrote the manuscript and revised the manuscript. All the authors approved the final manuscript.

Funding

The authors would like to thank the Ministry of Science and Technology of Taiwan for financially supporting this research under contract No. MOST 107-2221-E-218-032-MY2 and MOST 107-2218-E-492-007.

Availability of data and materials

The authors declare that the materials and data are promptly available to readers without undue qualifications in material transfer agreements. All data generated in this study are included in this article.

Competing interests

The authors declare that they have no competing interests.

Received: 22 January 2019 Accepted: 25 July 2019

Published online: 16 August 2019

References

- Adachi M, Karaki T, Miyamoto W (1999) Surface acoustic wave properties of $\text{La}_3\text{Ga}_5\text{SiO}_{14}$ (LANGASITE) single crystals. *Jpn J Appl Phys* 38:3283
- Takeda H, Shimamura K (1996) Growth and characterization of $\text{La}_3\text{Nb}_{0.5}\text{Ga}_{5.5}\text{O}_{14}$ single crystals. Takuya Kohno and Tsuguo Fukuda, *J Crystal Growth* 169:503
- Boutahraoui B, Nehari A, Boy J, Vacheret X, Allani M, Cabane H, Dumortier M, Derbal M, Lebbou K (2017) LGT ($\text{La}_3\text{Ga}_{5.5}\text{Ta}_{0.5}\text{O}_{14}$) langatate bulk crystal grown from the melt by Czochralski technique and characterization. *Opt Mater* 65:103
- Fritze H, Tuller HL (2001) Langasite for high-temperature bulk acoustic wave applications. *Appl Phys Lett* 78:976
- Zheng P, Greve DW, Oppenheim IJ (2013) Langasite surface acoustic wave gas sensors: modeling and verification. *IEEE Trans Ultrason Ferroelectr Freq Control* 60:579
- Pereira da Cunha M, Malocha DC, Adler EL, Casey KJ (2002) Surface and pseudo surface acoustic waves in langatate: predictions and measurements. *IEEE Trans Ultrason Ferroelectr Freq Control* 49(9):1291
- Wu S, Yan GJ, Lee MS, Ro RY, Chen KI (2007) Sputtering ZnO films on langasite and its saw properties. *IEEE Trans Ultrason Ferroelectr Freq Control* 54(12):2456
- Long C, Li T, Fan H, YunWu LZ, Li Y, Xiao L, Li Y (2016) Li-substituted $\text{K}_0.5\text{Na}_0.5\text{NbO}_3$ -based piezoelectric ceramics: crystal structures and the effect of atmosphere on electrical properties. *J Alloys Compd* 658:839e847
- Liu Z, Fan H, Zhao Y, Dong G (2016) Optical and tunable dielectric properties of $\text{K}_0.5\text{Na}_0.5\text{NbO}_3$ - SrTiO_3 ceramics. *J Am Ceram Soc* 99:146–151
- Lu D, Xu T, Yu H, Fu Q, Zhang H, Segonds P, Boulanger B, Zhang X, Wang J (2016) Acentric langanite $\text{La}_3\text{Ga}_{5.5}\text{Nb}_{0.5}\text{O}_{14}$ crystal: a new nonlinear crystal for the generation of mid-infrared parametric light. *Optics Express* 24(16):17603
- Guo F, Lu D, Segonds P, Debray J, Yu H, Zhang H, Wang J, Boulanger B (2018) Phase-matching properties and refined Sellmeier equations of $\text{La}_3\text{Ga}_{5.5}\text{Nb}_{0.5}\text{O}_{14}$. *Opt Mater Express* 8(4):858
- Voda M, García Solé J, Jaque F, Vergara I, Kaminskii A, Mill B, Butashin A (1994) Fano antiresonances in the optical-absorption spectra of Cr^{3+} doped $\text{La}_3\text{Ga}_{5.5}\text{Nb}_{0.5}\text{O}_{14}$ and $\text{La}_3\text{Ga}_{5.5}\text{Ta}_{0.5}\text{O}_{14}$ crystals. *Phys Rev* B49:3755
- Demidovich AA, Shkadarevich AP, Batay LE, Kuzmin AN, Ryabtsev GI, Strek W, Kaminskii AA (1997) Nd: $\text{La}_3\text{Ga}_{5.5}\text{Nb}_{0.5}\text{O}_{14}$ laser properties under LD pumping. In: *Proc. SPIE 3176, Tunable Solid State Lasers*, pp 269–271
- Studart AR, Gonzenbach UT, Tervoort E, Gauckler LJ (2006) Processing routes to macroporous ceramics: a review. *J Am Ceram Soc* 89(6):1771
- Eom JH, Kim YW, Raju S (2013) Processing and properties of macroporous silicon carbide ceramics: a review. *J Asian Ceram Soc* 1:220
- Yu FP, Yuan DR, Duan XL, Kong LM, Shi XZ, Guo SY, Wang LH, Cheng XF, Wang XQ (2008) Citrate sol-gel method to prepare nanoparticles of a piezoelectric crystal material: $\text{La}_3\text{Nb}_{0.5}\text{Ga}_{5.5}\text{O}_{14}$ at low temperature. *J Alloy and Compd* 459:L1–L4
- Kong H, Wang J, Zhang H, Yin X (2006) Growth and characterization of $\text{La}_3\text{Ga}_{5.5}\text{Nb}_{0.5}\text{O}_{14}$ crystal. *J Cryst Growth* 292:408
- Mill BV, Butashin AV, Kodzhabagian GG, Belokoneva EL, Belov NV (1982) Modified rare earth gallates with $\text{Ca}_3\text{Ga}_2\text{Ge}_4\text{O}_{14}$ structure. *Doklady Akademii Nauk SSSR* 264:1385
- Qiu S, Fan H, Zheng X (2007) $\text{Pb}(\text{Zr}_{0.95}\text{Ti}_{0.05})\text{O}_3$ powders synthesized by Pechini method: effect of molecular weight of polyester on the phase and morphology. *J Sol-Gel Sci Techn* 42:21
- Qiu S, Zheng X, Gao C, Gan X, Chen J, Yang C, Fan H (2009) $\text{Pb}(\text{Zr}_{0.95}\text{Ti}_{0.05})\text{O}_3$ powders and porous ceramics prepared by one-step pyrolysis process using non-aqueous Pechini method. *Ceram Inter* 35:733
- Qiu S, Fan H, Yang C, Chen J (2007) Porous $\text{Pb}(\text{Zr}_{0.95}\text{Ti}_{0.05})\text{O}_3$ ceramics from chemically prepared powders without pore formers. *J Am Ceram Soc* 10:3293
- Hsiao YJ, Chang YH, Chang YS, Fang TH (2007) Low-temperature preparation of $\text{Ba}_5\text{Nb}_4\text{O}_{15}$ ceramics through a sol-gel process. *J Am Ceram Soc* 97:2287
- Upadhyay RH, Agrekar AP, Deshmukh RR (2014) Characterization, dielectric and electrical behaviour of BaTiO_3 nanoparticles prepared via titanium(IV) triethanolaminate isopropoxide and hydrated barium hydroxide. *Bull Mater Sci* 37:481
- Lai WH, Teoh LG, Su YH, Shieh J, Hon MH (2007) Effect of calcination on crystallinity for nanostructured development of wormhole-like mesoporous tungsten oxide. *J Am Ceram Soc* 90:4073
- Dirksen GJ, Hoffman ANJM, van de Bout TP, Laudy MPG, Blasse G (1991) Luminescence spectra of pure and doped GaBO_3 and LiGaO_2 . *J Mater Chem* 1:1001
- Hsiao YJ, Liu CW, Dai BT, Chang YH (2009) Sol-Gel synthesis and the luminescent properties of CaNb_2O_6 phosphor powders. *J Alloy Compd* 475:698
- Shi S, Wang P, Cui J, Sun Z (2018) Microstructure and doping/temperature-dependent photoluminescence of ZnO nanospears array prepared by hydrothermal method. *Nanoscale Res Lett* 13:223
- Liu X, Huang X, Li J, Yadav SK, Gleiter H, Kong H, Feng T, Fuchs H (2016) Observation of intrinsic emission in $\beta\text{-BiNbO}_4$ available for excitation of both UV light and high energy irradiation. *Phys Chem Chem Phys* 18:23702
- Zhang A, Lü M, Wang S, Zhou G, Wang S, Zhou Y (2007) Novel photoluminescence of SrZrO_3 nanocrystals synthesized through a facile combustion method. *J Alloy Compd* 433:L7

Publisher's Note

Springer Nature remains neutral with regard to jurisdictional claims in published maps and institutional affiliations.

Submit your manuscript to a SpringerOpen® journal and benefit from:

- Convenient online submission
- Rigorous peer review
- Open access: articles freely available online
- High visibility within the field
- Retaining the copyright to your article

Submit your next manuscript at ► [springeropen.com](https://www.springeropen.com)